Design of an Adaptive Interference Reduction System for Nerve-Cuff Electrode Recording

Andreas Demosthenous, *Member, IEEE*, John Taylor, *Member, IEEE*, Iasonas F. Triantis, Robert Rieger, *Student Member, IEEE*, and Nick Donaldson

***Abstract*—This paper describes the design of an adaptive control system for recording neural signals from tripolar cuff electrodes. The control system is based on an adaptive version of the true-tripole amplifier configuration and was developed to compensate for possible errors in the cuff electrode balance by continuously adjusting the gains of the two differential amplifiers. Thus, in the presence of cuff imbalance, the output signal-to-interference ratio is expected to be significantly increased, in turn reducing the requirement for post-filtering to reasonable levels and resulting in a system which is fully implantable. A realization in 0.8-μm CMOS technology is described and simulated and preliminary measured results are presented. Gain control is achieved by means of current-mode feedback and many of the system blocks operate in the current-mode domain. The chip has a core area of 0.4 mm^2 and dissipates 3 mW from $\pm$ 2.5 V power supplies. Measurements indicate that the adaptive control system is expected to be capable of compensating for up to $\pm 5\%$ errors in the tripolar cuff electrode balance.**

***Index Terms*—Analog signal processing, cuff electrodes, implantable biomedical circuits, true tripole.**

I. Introduction

A MAJOR challenge in neuroprosthetics is to use naturally-occurring electroneurogram (ENG) signals to provide sensory feedback to artificial devices. Possible applications include correction of foot drop, hand grasp in tetraplegic patients, and bladder voiding [1]–[6]. The most chronically stable and safe method to record neural signals is by means of implanted cuffs fitted with electrodes and placed around nerve bundles [7]. Unfortunately, the ENG signal recorded using electrode cuffs is on the order of a few microvolts, whereas interfering signals can have much larger amplitudes [4], [8]. One source of interference, of millivolt amplitudes, is the electromyographic (EMG) potentials generated by excited muscles near the cuff. Various methods have been suggested to overcome this difficulty, mostly based on the use of multiple electrode structures within the cuff [7]–[11].

Manuscript received June 10, 2002; revised October 14, 2003. This work was supported by the United Kingdom Engineering and Physical Sciences Research Council (EPSRC) under Grant GR/M88990. This paper was recommended by Associate Editor G. Cauwenberghs.

A. Demosthenous, I. F. Triantis, and R. Rieger are with the Department of Electronic and Electrical Engineering, University College London, London WC1E 7JE, U.K. (e-mail: a.demosthenous@ee.ucl.ac.uk).

J. Taylor is with the Department of Electronic and Electrical Engineering, University of Bath, Bath BA2 7AY, U.K.

N. Donaldson is with the Department of Medical Physics and Bioengineering, University College London, London WC1E 6JA, U.K.

Digital Object Identifier 10.1109/TCSI.2004.823677

One of the simplest types of nerve cuff is a split cylinder containing three equally spaced ring electrodes embedded in the wall. Usually the two outer electrodes are connected to one input of a differential amplifier and the remaining central electrode is connected to the second input. This arrangement is termed the *quasi-tripole* [9]. Although the *monopolar* [10] arrangement (i.e., a single electrode placed centrally in the cuff with a remote indifferent electrode) produces a large-amplitude ENG signal, the differential arrangement of the quasi-tripole is preferred as it offers greater EMG rejection. As a result, the quasi-tripole has been used in a number of experimental studies and functional electrical stimulation applications [8], [9]. Unfortunately, EMG rejection by the quasi-tripole relies on symmetry in geometry and tissue resistivity, which will only be an approximation, at least due to manufacturing tolerances.

An alternative configuration, termed the *true tripole* [11], employs the same split cylinder and three electrode rings as the quasi-tripole. However, in this arrangement, the two outer electrodes are not shunted together but are connected to two separate differential amplifiers. The center electrode is then connected to the remaining input on both amplifiers. The outputs from the differential amplifiers are then summed in a third amplifier. One benefit of this arrangement is that the ENG signal recorded is about twice that in the quasi-tripole. On the other hand, it is much more sensitive to asymmetry, in geometry or tissue impedance, than the quasi-tripole.

In the past, attempts have been made to separate the ENG and EMG signals by filtering, since the peaks of their power-spectral densities differ by about an order of magnitude (although the spectra overlap considerably). This frequency-domain approach has involved the use of very high-order digital filters, which are not suitable for implanted devices [2]. An alternative approach to minimizing EMG artefacts in nerve-cuff electrode recording has recently been proposed [12]. This is based on a feedback control mechanism, which adaptively tunes the gains of two differential amplifiers in a true-tripole configuration to compensate for possible errors in the cuff electrode balance. The approach takes advantage of the fact that over the dimensions of a typical cuff (about 2–3 cm) there is no significant phase variation in the EMG signal. As a result, the feedback control system is only required to adapt to amplitude variations in the EMG. Although the EMG cannot be completely eliminated, the requirement for postfiltering is reduced to manageable levels resulting in a system that is implantable. Increasing the signal-to-interference (S/I) ratio of the ENG signal before digitization relaxes the resolution requirement of the analog-to-digital (A/D) conversion and other digital parts of the transcutaneous link.

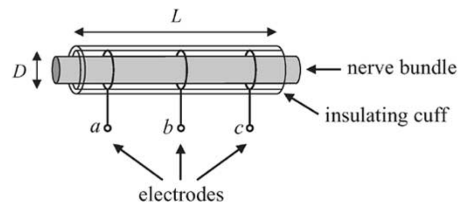

Fig. 1. Insulating cuff and tripolar electrode assembly fitted to a nerve bundle.

This paper describes the design of the adaptive control system using analog signal-processing circuit techniques and fabricated in 0.8-μm CMOS technology. Preliminary measurements indicate that the system is expected to be capable of compensating for about $\pm 5\%$ imbalance errors resulting from impedance mismatch between the two halves of a tripolar cuff. The fabricated chip has a core area of 0.4 mm^2 and dissipates 3 mW from $\pm$2.5-V power supplies. Amplifier variable gain control is achieved by means of current feedback.

The rest of the paper is organized as follows. Section II describes the basic principles of the cuff and explains the true-tripole amplifier configuration, while Section III provides a description and mathematical analysis of the adaptive control system. Section IV describes the circuit design, while simulated and preliminary measured results are presented in Sections V and VI, respectively. Finally, conclusions are drawn in Section VII.

II. Theory

Fig. 1 shows a cylindrical cuff fitted to a nerve bundle. In this example, the insulating cuff of length L and internal diameter D is shown fitted with three equally-spaced circular electrodes (a, b, c). L is typically 2–3 cm while D is typically 1–2 mm depending on the diameter of the nerve. To a first approximation, the nerve bundle is an insulator, while the space between the nerve and the cuff is filled with a conducting fluid and later fibrous capsule.

The ENG signal results from the action potentials, propagating along the nerve fibers, which cause small action currents to flow through the fiber membranes into the extrafascicular medium. Confinement within an insulating cuff causes the local impedance to be higher than outside the cuff, so that the action currents give rise to measurable potentials between the electrodes. The interelectrode spacing must be approximately equal to the wavelength of the transmembrane action potential, which is about 3 cm for a 10-μm fiber diameter.

The second important function of the cuff is that, as a uniform insulating tube, any externally applied potential differences, between the ends, will produce a linear gradient inside. This *linearization* [13] is shown diagrammatically in Fig. 2 together with the basic lumped-impedance model of the cuff [8], [14]. In this model, Z_{t1} and Z_{t2} represent the tissue impedances inside the cuff, Z_{t0} is the tissue impedance outside the cuff, Z_{e1}, Z_{e2}, and Z_{e3} are the electrode-tissue contact impedances, $I_{\rm EMG}$ is the interfering EMG current that flows in the cuff, and $I_{\rm ENG1} I_{\rm ENG2}$ are the ENG currents. Given the linear gradient of the EMG potential inside the cuff and equally-spaced tripolar electrodes, the residual EMG at the output from either the quasi-

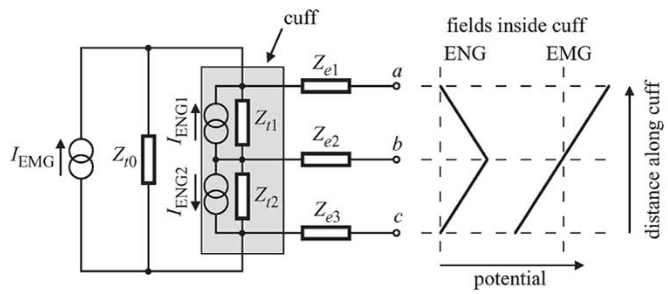

Fig. 2. Lumped-impedance model of the cuff and idealized ENG and EMG potentials inside the cuff. Typical impedance values: $Z_{t0} = 100\ \Omega$, $Z_{t1,2} = 2\ \mathrm{k}\Omega$, $Z_{e1,2,3} = 1\ \mathrm{k}\Omega$.

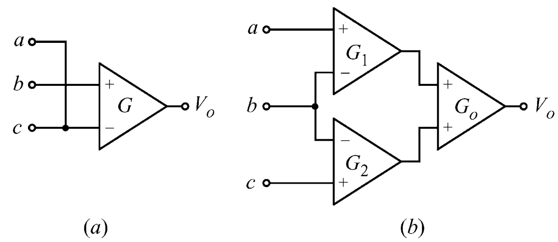

Fig. 3. Tripolar amplifier recording configurations. (a) Quasi-tripole. (b) True tripole.

or true-tripole amplifier configurations (Fig. 3) will ideally be zero. However, in practice, the various cuff impedances are subject to significant variation with time for two main reasons: 1) changes in the nerve-cuff impedances due to tissue regrowth inside the cuff after implantation and 2) manufacturing tolerances. This degrades the performance of both amplifier configurations, although the effect of impedance mismatch on the true tripole is more pronounced [15].

In the case of the true tripole, the residual EMG at its output is given by [14]

$$V_{o(\rm EMG)} = I_{\rm EMG}\left(\frac{Z_{t0}(G_1 Z_{t1} - G_2 Z_{t2})}{Z_{t0} + Z_{t1} + Z_{t2}}\right) \tag{1}$$

where G_1 and G_2 are the gains of the input differential amplifiers in Fig. 3(b). Note that (1) can be made zero by adjusting G_1 and G_2, irrespective of the cause of the tissue impedance mismatch. Nevertheless, the interference cancellation is very sensitive to the various parameter values (especially after implantation), emphasizing the need for some form of *adaptive* adjustment of G_1 and G_2.

III. Adaptive Control System

A simplified block diagram of the proposed control system is shown in Fig. 4. It consists of a true-tripole amplifier configuration in which the gains of the input differential amplifiers (G_1 and G_2) have been made variable, controllable by the differential feedback voltages $+V_f$ and $-V_f$. The system operates by first obtaining the *moduli* of the outputs of G_1 and G_2 and comparing them to determine which is the largest. The difference between the resulting signals is integrated by the differential-output integrator block. The feedback voltages $+V_f$ and $-V_f$ adjust the amplifier gains to compensate for the difference

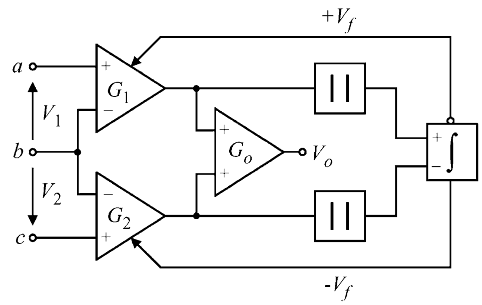

Fig. 4. Elements of an adaptive control system for nerve-cuff electrode recording.

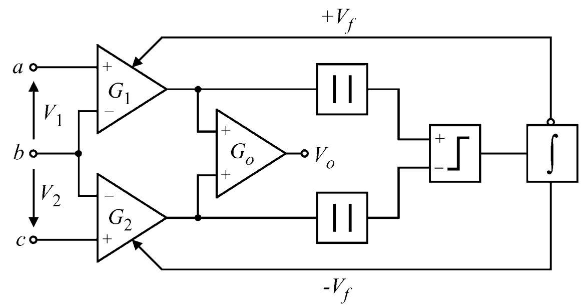

Fig. 5. Improved configuration of the adaptive control system.

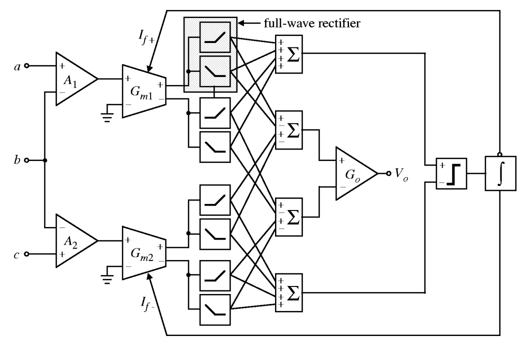

Fig. 6. Complete block diagram of the adaptive control system.

between the inputs. For the purpose of analysis, the variable gain amplifiers are modeled as

$$\begin{aligned} G_1 &= G(1 - aV_f) \\ G_2 &= G(1 + aV_f) \end{aligned} \tag{2}$$

where $V_f(t)$ is the feedback voltage, a is the feedback-loop gain coefficient (in V^{-1}), and G (mean variable amplifier gain) is taken to be unity. Assuming that the inputs to the two variable gain amplifiers are solely EMG signals[1] described by step functions at the origin with final values V_1 and V_2, the system behavior is defined by the first-order differential equation

$$\frac{dV_f(t)}{dt} + \frac{\alpha}{\tau}(|V_1| + |V_2|)V_f(t) + \frac{1}{\tau}(|V_2| - |V_1|) = 0 \tag{3}$$

with the solution [16]

$$V_f(t) = \frac{1}{\alpha}\left(\frac{|V_1| - |V_2|}{|V_1| + |V_2|}\right)\left(1 - e^{-[\alpha(|V_1|+|V_2|)/\tau]t}\right) \tag{4}$$

where τ is the time constant of the integrator. The effective time constant of the system is $\tau/[\alpha(|V_1| + |V_2|)]$, which depends not only on the system constants but also on the magnitudes of the input voltages. Thus, a reasonable estimate of the *settling time* to about 1% is

$$t_s = \frac{5\tau}{a}\left(\frac{1}{|V_1| + |V_2|}\right) \tag{5}$$

which can be very slow for small inputs. Once the state variables have settled, the ENG signal can be extracted from the node marked V_o in Fig. 4 since the EMG signals will cancel at that node.

In order to avoid the problem of the very slow settling for small inputs, the alternative form shown in Fig. 5 can be employed. In this system, the integrator is preceded by a comparator which provides a voltage output of fixed value $\pm V_e$, the sign depending on which input is the larger. As in the previous case, for step inputs, and assuming that the comparator gain is approximated by $V_e/\left(|V_1| - |V_2|\right)$, a first-order analysis leads to the expression for the settling time

$$t_s = \frac{5\tau}{aV_e}\left(\frac{|V_1| - |V_2|}{|V_1| + |V_2|}\right) \tag{6}$$

where the sign of V_e is positive if $|V_1| > |V_2|$ and negative if $|V_2| > |V_1|$. Note that in this case, the settling time depends on the constants α, τ, and V_e, in addition to the term on the right of the expression. This term is a *measure of similarity* between the inputs and is zero when they are perfectly matched. A reasonable upper bound on the difference between $|V_1|$ and $|V_2|$ is $\pm 10\%$, corresponding to a value of 1/10 for the term in the brackets. Thus, unlike the previous case, there is virtually no dependence on the absolute value of the inputs. As a result, this approach was adopted for the design described in this paper.

[1]The ENG is about three orders of magnitude smaller than the EMG and hence may be ignored.

IV. Circuit Design

The adaptive control system was realized using analog signal-processing circuit techniques. Some of the system building blocks (e.g., rectifiers) operate in the *current-mode* domain [17] for easy manipulation of signals. The complete block diagram of the control system is shown in Fig. 6. In order to simplify the design of the control system it is preceded by two *preamplifiers* each with a fixed gain of about 100 optimized for low noise performance. This ensures that the signal levels at the input to the variable gain stages are sufficiently large that low noise design is not necessary in these and subsequent parts of the system. The preamplifier design was explicitly described in [18] and hence is not described in this paper. For convenience its key measured performance parameters are summarized in Table I. Note particularly the required noise performance, for example, the total input-referred voltage noise in a bandwidth 1Hz–10 kHz, which is a reflection of the small ENG signal levels obtained from nerve cuffs. It should be noted that although the preamplifier in [18] was designed using bipolar n-p-n transistors in a BiCMOS process for optimum noise performance, a CMOS solution is also possible by employing lateral p-n-p transistors but with a somewhat worse noise performance.

TABLE I
MEASURED PARAMETERS OF THE PREAMPLIFIER [18]

Parameter	Value
Power supply	± 2.5 V
Power consumption	1.3 mW
Circuit area	0.3 mm^2
Gain	110
–3 dB frequency	14 kHz
CMRR @ 1 kHz	82 dB
PSRR @ 1 kHz V_{DD} V_{SS}	 42 dB 54 dB
Total input-referred noise voltage PSD @ 1 Hz @ 1 kHz	 $11.5\,\mathrm{nV}/\sqrt{\mathrm{Hz}}$ $3.3\,\mathrm{nV}/\sqrt{\mathrm{Hz}}$
Total input-referred noise current PSD @ 1Hz @ 1kHz	 $34\,\mathrm{pA}/\sqrt{\mathrm{Hz}}$ $1.8\,\mathrm{pA}/\sqrt{\mathrm{Hz}}$
Total input-referred r.m.s. noise voltage (1 Hz – 10 kHz)	290 nV
Residual input DC base current	120 nA

As shown in Fig. 6, each variable gain stage (G_{m1} and G_{m2}) is realized by a balanced operational transconductance amplifier (OTA) whose differential-output currents feed into full-wave rectifiers (made up of half-wave rectifiers). For EMG comparison and hence OTA gain adjustment, the output currents of the rectifiers are summed as shown, before being applied to the comparator-integrator which generates the differential feedback currents I_f+ and I_f-. For ENG reconstruction, the output currents of the rectifiers are summed and subtracted as shown, before being applied to the output stage amplifier. The circuit design details of the various building blocks are described below.

A. Variable Gain OTAs

The input to each half of the adaptive control system consists of the superposition of two signals (ENG plus EMG), which differ from each other in both amplitude and spectral content. The amplitudes of the EMG and ENG signals after preamplification are typically of the order of ± 50 mV and ± 100 μV, respectively. The control system must therefore have sufficient gain to amplify the ENG to a reasonable target amplitude while providing sufficient linearity to accommodate the EMG signal, at least in the parts of the system before the point at which the EMG is cancelled. In addition, the input stages must have a sufficient variable gain capability to cope with practical levels of cuff imbalance.

Each variable gain stage was realized by the balanced CMOS OTA circuit shown in Fig. 7. The use of an OTA is not only a simple way to implement a variable gain amplifier, the *transconductance gain* depending on the tail current, but the current output also simplifies the design of some of the succeeding stages. Essentially, the circuit consists of a pair of simple CMOS OTAs ($M1$–$M4$ and $M5$–$M8$) with inputs reversed. The sources of all the nMOS transistors are connected to a common node and so each pair operates with half the tail current (I_f). Hence, the *differential* transconductance of the circuit is twice that of each

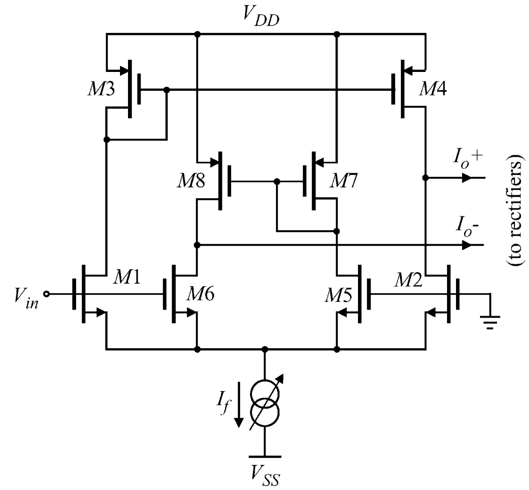

Fig. 7. CMOS balanced OTA variable gain stage.

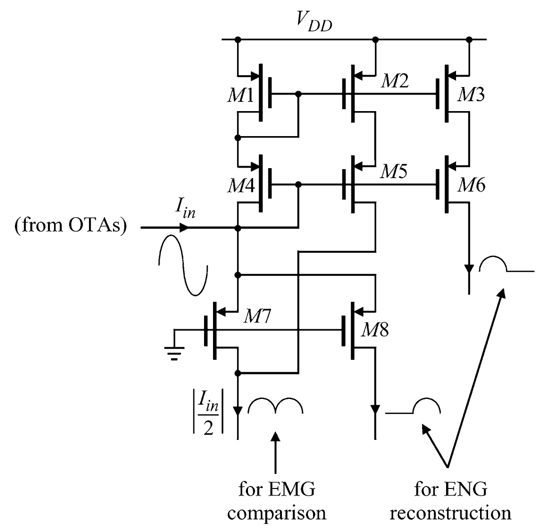

Fig. 8. Full-wave rectifier circuit.

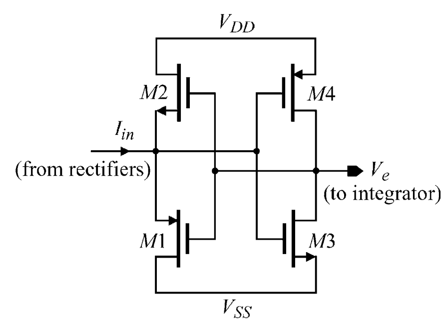

Fig. 9. Comparator circuit.

simple OTA. The use of a balanced structure cancels (to a first order) any errors due to asymmetry in the output currents I_o+ and I_o- for equal and opposite excursions of the input voltage (V_{in}). Operation in weak inversion is clearly attractive because it often leads to low-power designs, but this approach was impractical here due to the amplitude of the input EMG signal and the need for a fairly large transconductance gain to meet the overall gain requirement.

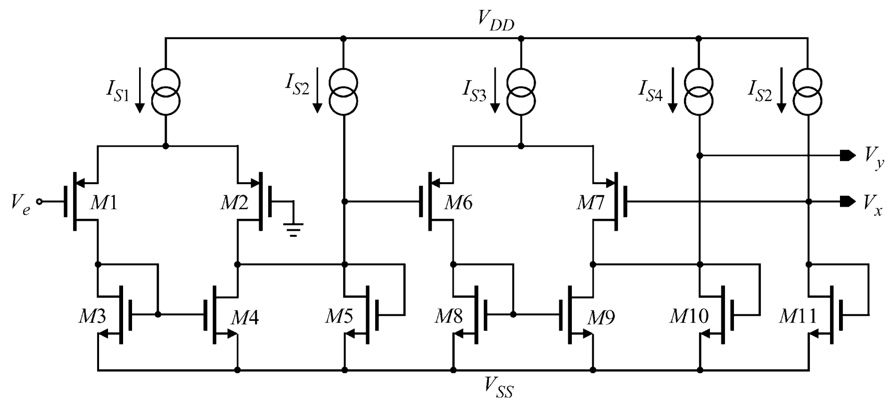

Fig. 10. First four stages of the integrator.

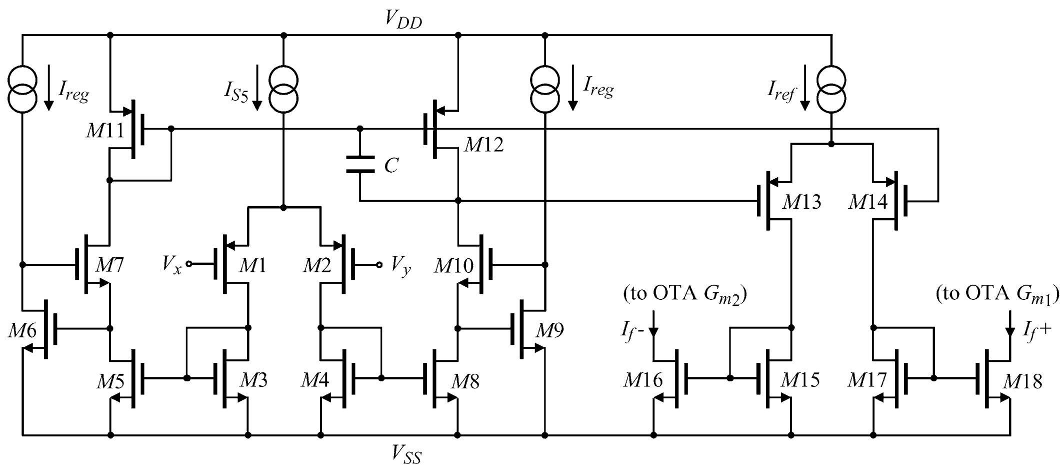

Fig. 11. Fifth stage of the integrator and generation of the feedback control currents.

In strong inversion and assuming matched transistors, the output current of a simple OTA is given by [17]

$$I_o = \sqrt{I_f k}V_{in}\sqrt{1 - \frac{k}{I_f}V_{in}^2}, \quad |V_{in}| \leq \sqrt{\frac{I_f}{2k}} \tag{7}$$

where $k = \mu C_{\text{ox}} W/2L$ is the transconductance parameter, W and L are the channel width and length of the input nMOS transistors, μ is the carrier mobility, and C_{ox} is the gate oxide capacitance per unit area. Its transconductance, G_m, is obtained by taking the derivative of (7) with respect to V_{in}, yielding

$$G_m = \frac{\sqrt{I_f k}\left[1 - \frac{2kV_{in}^2}{I_f}\right]}{\sqrt{1 - \frac{kV_{in}^2}{I_f}}}. \tag{8}$$

For $V_{in} \ll \sqrt{I_f/4k}$, (8) simplifies to

$$G_m = \sqrt{I_f k} \tag{9}$$

and in order to obtain a linear transconductance within 1%, it is required that [19]

$$|V_{in}| < 0.2\sqrt{\frac{I_f}{2k}}. \tag{10}$$

Thus, gain control can be implemented by varying I_f either side of its nominal value I_{fo}. Equation (2) may be rewritten as

$$G_m = \sqrt{I_{fo}k}\sqrt{1 \pm \frac{\Delta I_f}{I_{fo}}} \tag{11}$$

and for small excursions of the controlling tail current

$$G_m \cong G_{mo}\left(1 \pm \frac{\Delta I_f}{I_{fo}}\right) \tag{12}$$

which is of the form of (2).

Given the nature of the input signal after pre-amplification as discussed and taking 200 mV (pk–pk) as a reasonable ENG target amplitude for the system output, a nominal value for G_m of 200 μA/V (i.e., differential transconductance of 400 μA/V) was chosen. Given these constraints and allowing for a $\pm 10\%$ variation in V_{in}, (9) and (10) can be solved simultaneously for appropriate values of k and I_f.

B. Full-Wave Rectifiers

The rectifiers in Fig. 6 were realized by four current-mode full-wave rectifiers of the type shown in Fig. 8. This arrangement is derived from the current-squaring circuit described in [20], but with the dc bias current reduced to a very low level. The circuit consists of four parallel paths, two for each phase of the

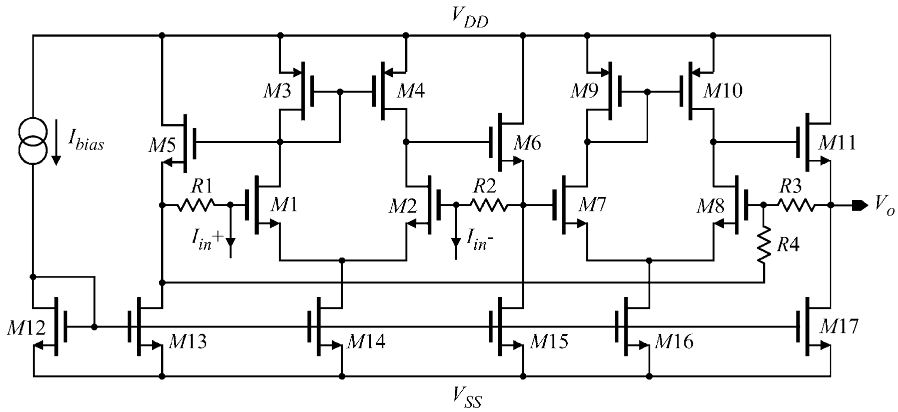

Fig. 12. Output stage.

input signal, which are summed or subtracted in pairs by means of simple nMOS current mirrors (not shown) according to the polarity signs at the input of each sum block (Σ) in Fig. 6. In the presence of a significant input current, the operating point of the circuit changes, resulting in either the pMOS mirror $M1$–$M6$ or the pMOS common-gate transistors $M7$ and $M8$ being turned off depending on the polarity of the input current. Although a small dc bias current flows when there is zero input current, once the circuit is driven by an input current of either polarity this current is turned off by the resulting change in operating point. In the design, this bias current was set to about 50 nA so that for a typical EMG input (after pre-amplification) of about ± 50 mV the resulting error is negligible.

C. Comparator

The comparator shown in Fig. 9 uses a CMOS inverter ($M3$, $M4$) to apply feedback around a pair of complementary source followers ($M1$, $M2$) [21]. As a result of the feedback, the input has a low impedance (in general), and is thus ideal for detecting the relative magnitudes of two competing input currents. On the other hand, the output of the inverter does not slew between the power supplies and so a quiescent current flows resulting in dc power dissipation. Fortunately, since in this application low-speed operation is required, the comparator transistors could be scaled to minimize power dissipation. The follower transistors have zero dc power dissipation.

D. Long Time-Constant Integrator

Given the static or very slowly time-varying nature of the imbalances mentioned in Section II, the integrator time-constant should be as long as possible. For practical reasons, a time-constant of 1 s was employed as a reasonable compromise between area and artefact suppression. The design of the integrator was based on the OTA-C approach operating in the weak inversion mode, and in order to achieve a very small transconductance a chain of transconductance-transimpedance ($g_m - 1/g_m$) stages were cascaded [22]. In total, three g_m and two $1/g_m$ stages were cascaded and the resulting *total* transconductance is given by

$$G_{mT} = g_{m1}\left(\frac{I_{S3}I_{S5}}{4I_{S2}I_{S4}}\right) \tag{13}$$

TABLE II
TRANSISTOR DIMENSIONS

Circuit	Transistor Label	W/L (μm/μm)
OTA (Fig. 7)	$M1$, $M2$, $M5$, $M6$	100/10
	$M3$, $M4$, $M7$, $M8$	200/5
Rectifier (Fig. 8)	$M1$, $M4$	200/2
	$M2$, $M3$, $M5-M8$	100/2
Comparator (Fig. 9)	$M1$, $M4$	5/2
	$M2$, $M3$	2/2
Integrator (Fig. 10)	$M1-M4$, $M6-M9$	10/5
	$M5$, $M10$, $M11$	90/5
Integrator (Fig. 11)	$M1-M10$	10/5
	$M11$, $M12$	6/6
	$M13$, $M14$	100/2
	$M15-M18$	20/10
Output stage (Fig. 12)	$M1$, $M2$, $M7$, $M8$	120/2
	$M3$, $M4$, $M9$, $M10$	20/2
	$M5$, $M6$	60/2
	$M12-M17$	20/5

TABLE III
RESULTS OF MONTE CARLO ANALYSIS FOR 200 RUNS. (S/I RATIO WITHOUT ADAPTIVE CANCELLATION $= 1/50$ OR -34 dB)

Percentage of Runs (%)	S/I ratio
9	≥ 4 (12 dB)
19	≥ 2 (6 dB)
34	≥ 1 (0 dB)
59	$\geq 1/2$ (-6 dB)
75	$\geq 1/3$ (-9.5 dB)
86	$\geq 1/4$ (-12 dB)
94	$\geq 1/5$ (-14 dB)
100	$> 1/6$ (-15 dB)

where g_{m1} is the transconductance of the first stage and I_{S1-S5} is the total current in each stage.

The circuit schematic of the first four stages of the integrator is shown in Fig. 10. Each transconductance stage is realized by a simple CMOS OTA ($M1$–$M4$ and $M6$–$M9$) while each transimpedance stage by a diode-connected nMOS transistor ($M5$ and $M10$). The extra diode-connected transistor $M11$ is used to obtain better balanced dc conditions. The last transconductance stage of the integrator shown in the left section of Fig. 11 is a symmetrical OTA ($M1$–$M12$) with regulated cascode nMOS

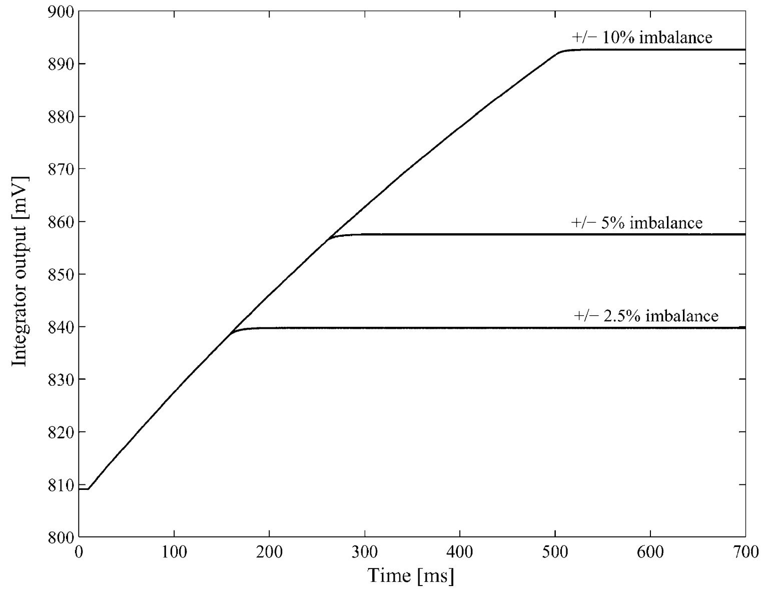

Fig. 13. System setting time for the EMG step signal as monitored at the output of the integrator for $|V_1| < |V_2|$. The step waveforms were applied at 10 ms.

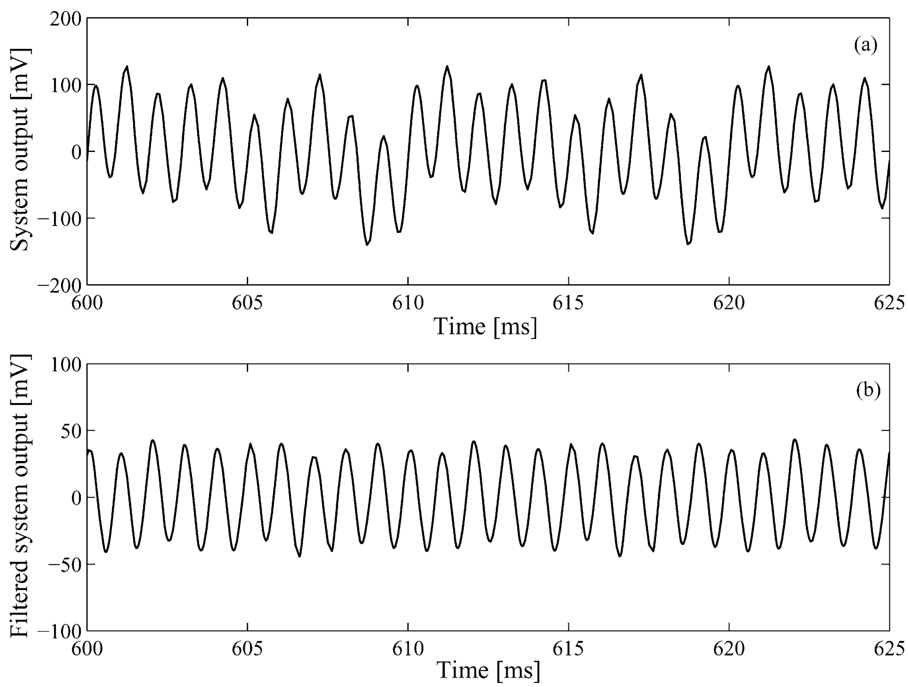

Fig. 14. Time-domain system output after setting for the sinusoidal inputs (10% imbalance). (a) Raw data. (b) After high-pass filter.

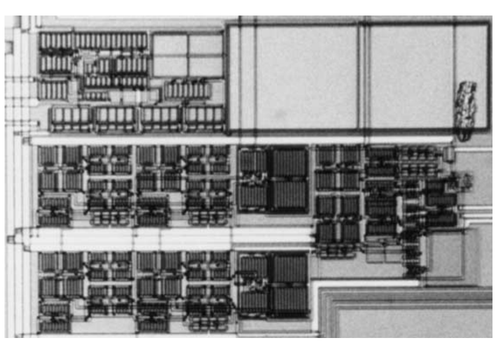

Fig. 15. Chip microphotograph (system core).

transistors biased by current sources I_{reg}. The integrating capacitor C (70 pF) is connected across the gate and drain of $M12$ which are low- and high-impedance points, respectively. Currents I_{S1}–I_{S5} in Figs. 10 and 11 are all in the nanoampere range, and these are derived from a single 10 μA bias current using step-down current mirrors (not shown). The integrator was designed to operate in an open-loop configuration [22]. Its time constant τ is given by $2r_oC$, where r_o is the resistance seen at the node connecting the drains of $M10$ and $M12$ in Fig. 11.

To generate the feedback control currents I_f+ and I_f- required to adjust the gains of the variable gain OTAs, the two sides of C are connected across the inputs of the pMOS differential pair $M13$ and $M14$ in Fig. 11. The values of I_f+ and I_f-

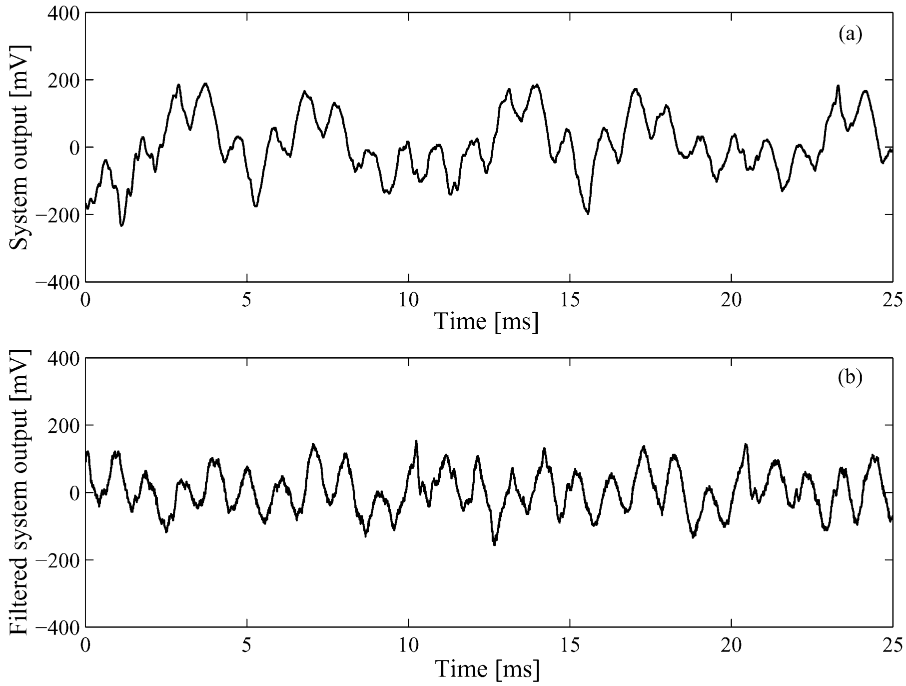

Fig. 16. Measured time-domain system output after setting for sinusoidal inputs ($\pm 10\%$ imbalance). (a) Raw data. (b) After high-pass filter.

are controlled by the externally defined reference current I_{ref} which has a nominal value of 200 μA.

E. Output Stage

The output stage is shown in Fig. 12. It consists of two stages: a transimpedance amplifier ($M1$–$M6$; nominal transimpedance 20 kΩ) cascaded with a voltage amplifier ($M7$–$M11$; voltage gain 115), together with some overall feedback. The total transimpedance of this system is therefore 2.3 MΩ. Given that the nominal differential transconductance of each balanced variable gain OTA is 400 μA/V, the overall ENG voltage gain is 420. With a bias current I_{bias} of 10 μA, the -3 dB frequency of this circuit is 750 kHz.

V. Simulated Results

The following simulation results were obtained using the Cadence Analog Artist toolkit, based on foundry parameters for the AMS 0.8-μm CMOS CYE process [23]. Transistor dimensions for the circuits described in Section IV are listed in Table II. Two pairs of waveforms were employed to represent the ENG and EMG signals. In all cases the ENG signal was simulated by a sinusoidal signal of frequency 1 kHz and peak amplitude 100 μV (i.e., a typical value after pre-amplification). The EMG signal was simulated by: 1) a step function of amplitude 50 mV and 2) a sinusoidal signal of frequency 100 Hz and peak amplitude 50 mV. The amplitudes of the composite waveforms, applied to the two inputs of the control system were then changed differentially to simulate the effects of cuff imbalance. The control system operated with power supplies of $\pm$2.5 V.

The use of the step function was intended to verify the setting time of the system as defined by (6) which for the current-mode design described in Section IV, modifies to

$$t_s = \frac{5 I_{ref} \tau}{4 g_L V_e} \left(\frac{|V_1| - |V_2|}{|V_1| + |V_2|} \right) \tag{14}$$

where g_L is the feedback loop transconductance, and all other symbols are as previously defined. Substituting for $V_e = 200$ mV, $I_{ref} = 200$ μA, $\tau = 1$ s, and $g_L = 260\mu$A/V into (14), for $\pm 10\%$ imbalance results in a value of t_s of 480 ms which agreed closely with the simulations (see Fig. 13).

For the sinusoidal EMG signal, the time-domain output of the system is shown in Fig. 14(a) (captured after setting) for 10% imbalance. As can be seen, the output consists of the ENG signal (amplified to about 200 mV pk–pk) and some residual EMG artefact. The resulting S/I ratio, measured as the ratio of the ENG amplitude to the largest residual EMG spectral component, is about 4.5 (13 dB). This should be compared with a ratio of 1/500 (-54 dB) at the electrodes, and with a ratio of 1/50 (-34 dB) after the true-tripole configuration [Fig. 3(b)] with the input differential amplifiers set for equal gain. Fig. 14(b) shows the same waveform after passage through a third-order Butterworth high-pass filter with cutoff frequency 500 Hz (note 6-dB insertion loss). This removes a significant proportion of the residual EMG artefact resulting in a further 8.5-dB improvement in the S/I ratio.

To investigate the sensitivity of the circuit design to process and transistor mismatch variations, Monte Carlo analysis was performed using process and mismatch parameter variation statistics provided by the foundry. The results for a trial of 200 runs for the sinusoidal EMG and ENG signals ($\pm 10\%$ imbalance) are summarized in Table III. For 59% of the trials the S/I ratio was better than 1/2 (-6 dB) and none of the trials dropped below a

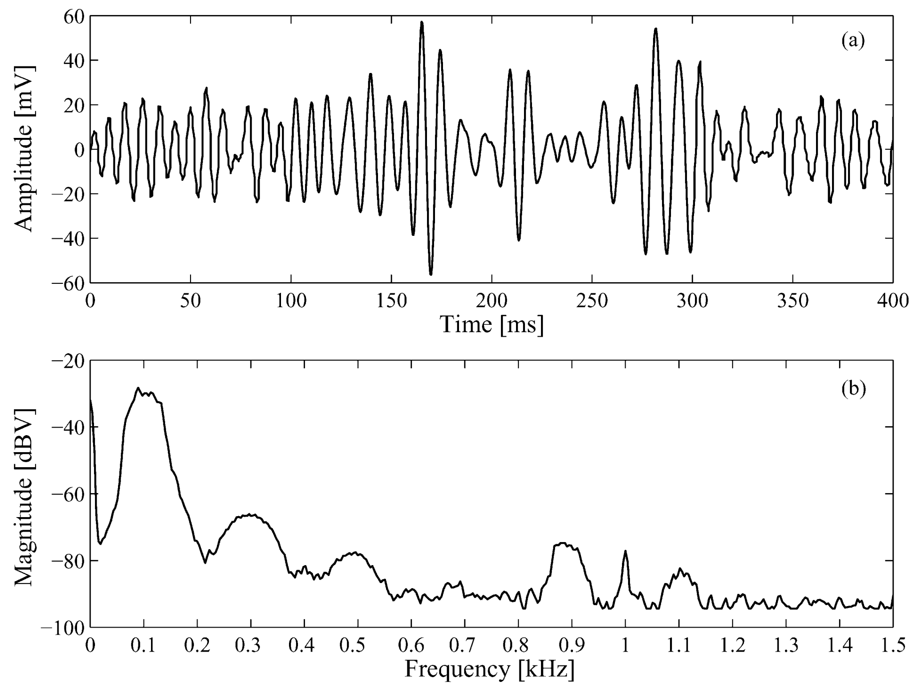

Fig. 17. System input signal made up of the superposition of an arbitrary signal representing the EMG plus sinusoid ENG. (a) Time domain. (b) Spectrum.

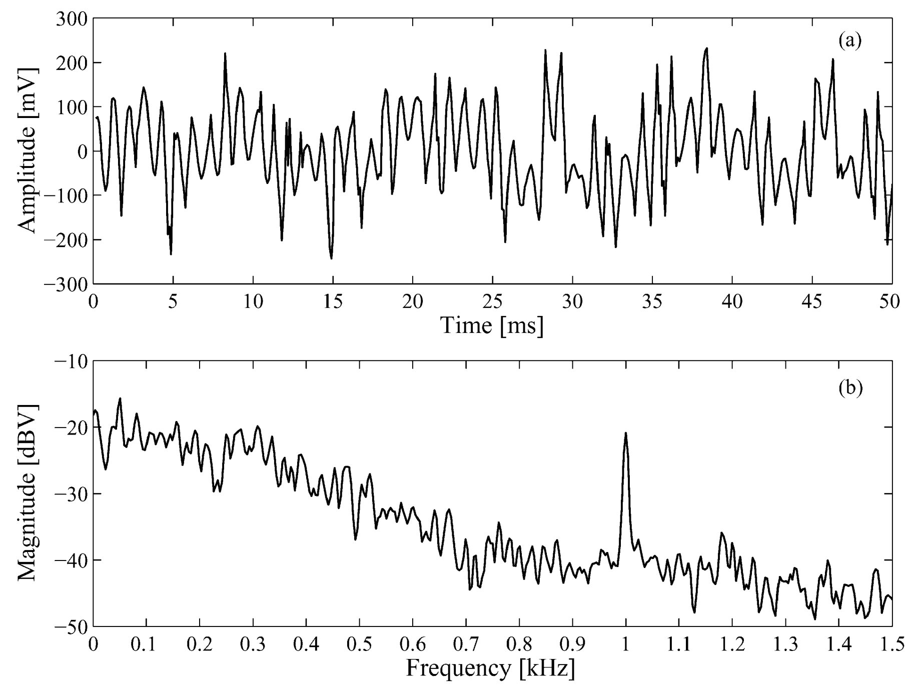

Fig. 18. Measured system output for the input waveform in Fig. 17 (-5% imbalance). (a) Time domain. (b) Spectrum.

S/I ratio of 1/6 (−15.5 dB) which is still a 18.5-dB improvement compared to the standard true-tripole amplifier configuration with the same level of imbalance.

VI. Measured Results

Two complete systems (excluding the preamplifiers) were fabricated in the AMS 0.8-μm CMOS CYE process. System A was a test structure intended to allow dc conditions to be examined while System B was intended for operation under signal conditions for transient analysis. The chip microphotograph (System B core) is depicted in Fig. 15.

Measurements were carried out on System A to investigate the linearity of the variable gain OTA and its tuning capability, the precision of the full-wave rectifiers, the resolution of the comparator and the time-constant of the integrator. System B was initially tested with superimposed sinusoidal signals identical to those used in the simulations in Section V. Fig. 16(a)

TABLE IV
MEASURED PARAMETERS OF ADAPTIVE CONTROL SYSTEM

Parameter	Value
Technology	0.8 μm CMOS
Active area	0.4 mm^2
Power supply	± 2.5 V
Power consumption	3 mW
ENG path gain	52.5 dB
Imbalance correction range	~ ± 5%
Setting time (step inputs)	
± 2.5% imbalance	130 ms
± 5% imbalance	255 ms

shows the system output for -5% imbalance. As can be seen the control system can successfully extract and amplify the tiny ENG sinusoidal signal. The residual EMG artefact present in Fig. 16(a) is attributed to circuit offsets and mismatch and to the fact that the feedback loop is not pure dc. The artefact can be minimized by post-filtering as shown in Fig. 16(b) (first-order high-pass filter with a cutoff frequency of 500 Hz). System B was subsequently tested with an arbitrary signal (representing the EMG) designed to have a spectrum which is a better approximation to a real EMG signal than a simple sinusoid. The arbitrary signal was generated from band-limited white noise scaled to the appropriate EMG amplitudes. The time-domain plot of the resulting superimposed input signal (arbitrary EMG plus sinusoid ENG) and its spectrum are shown in Fig. 17. Despite the fact that the frequency spectra of the two signals overlap with frequency components of the EMG reaching even higher frequencies than the ENG and for -5% imbalance, the control system extracts and amplifies the ENG signal as depicted in Fig. 18. The main measured parameters of the adaptive control system are summarized in Table IV. A future design will address greater imbalance correction and better output S/I.

VII. CONCLUSION

The circuit design of an adaptive control system for the recording of ENG signals from a true-tripolar cuff electrode arrangement has been described. The control system has been developed to enable static and slow time-varying errors in the electrode balance such as those due to manufacturing tolerance and tissue re-growth to be cancelled adaptively. As a result, full advantage can be taken of the properties of the true-tripole configuration without suffering from its high sensitivity to imbalance. Furthermore, the described implementation is very economical in terms of size and power dissipation, features that make it very attractive for the design of a low-power, fully implantable ENG amplifier. The operation of the control system has been demonstrated both by simulations and preliminary measurements from an integrated realization.

REFERENCES

[1] M. K. Haugland and T. Sinkjaer, "Cutaneous whole nerve recordings used for correction of footdrop in hemiplegic man," *IEEE Trans. Rehab. Eng.*, vol. 3, pp. 307–317, Dec. 1995.

[2] B. Upshaw and T. Sinkjaer, "Digital signal-processing algorithms for the detection of afferent nerve activity recorded from cuff electrodes," *IEEE Trans. Rehab. Eng.*, vol. 6, pp. 172–181, June 1998.

[3] M. Haugland, A. Lickel, J. Haase, and T. Sinkjaer, "Control of FES thumb force using slip information obtained from the cutaneous electroneurogram in quadriplegic man," *IEEE Trans. Rehab. Eng.*, vol. 7, pp. 215–227, June 1999.

[4] M. K. Haugland, J. A. Hoffer, and T. Sinkjaer, "Skin contact force information in sensory nerve signals recorded by implanted cuff electrodes," *IEEE Trans. Biomed. Eng.*, vol. 2, pp. 18–28, Mar. 1994.

[5] T. Sinkjaer, M. K. Haugland, and J. Haase, "Natural neural sensing and artificial muscle control in man," *Exp. Brain Res.*, vol. 98, pp. 542–545, 1994.

[6] S. Jezernik and T. Sinkjaer, "Detecting sudden bladder pressure increases from the pelvic nerve afferent activity," in *Proc. 20th Int. Conf. IEEE Engineering Medicine and Biology Soc.*, vol. 5, Hong Kong, 1998, pp. 2532–2535.

[7] J. J. Struijk, M. Thomsen, J. O. Larsen, and T. Sinkjaer, "Cuff electrodes for long-term recording of natural sensory information," *IEEE Eng. Med. Biol. Mag.*, vol. 18, pp. 91–98, May/June 1999.

[8] Z. M. Nikolić, D. B. Popović, R. B. Stein, and Z. Kenwell, "Instrumentation for EMG recordings in FES systems," *IEEE Trans. Biomed. Eng.*, vol. 41, pp. 703–706, July 1994.

[9] R. Stein, C. Davis, J. Jhamanda, A. Mannard, and T. Nichols, "Principles underlying new methods for chronic neural recording," *J. Can. Sci. Neurol.*, vol. 2, pp. 235–244, 1975.

[10] M. Thomsen, J. J. Struijk, and T. Sinkjaer, "Artifact reduction with monopolar nerve-cuff recording electrodes," in *Proc. 18th Int. Conf. IEEE Engineering Medicine and Biology Soc.*, vol. 1, Amsterdam, Netherlands, 1996, pp. 367–368.

[11] C. Pflaum, R. R. Riso, and G. Wiesspeiner, "Performance of alternative amplifier configurations for tripolar nerve-cuff recorded ENG," in *Proc. 18th Int. Conf. IEEE Engineering Medicine and Biology Soc.*, vol. 1, Amsterdam, Netherlands, 1996, pp. 375–376.

[12] M. Rahal, J. Winter, J. Taylor, and N. Donaldson, "Adaptive interference reduction (AIR) in cuff electrode recordings," in *Proc. 1st IEEE Joint BMES/EMBS Conf.*, vol. 1, Atlanta, GA, 1999, p. 419.

[13] J. J. Struijk and M. Thomsen, "Tripolar nerve-cuff recordings: Stimulus artefact, EMG, and the recorded nerve signal," in *Proc. 17th Int. Conf. IEEE Engineering Medicine and Biology Soc.*, vol. 2, Montreal, Canada, 1995, pp. 1105–1106.

[14] M. Rahal, J. Winter, J. Taylor, and N. Donaldson, "An improved configuration for the reduction of EMG in electrode cuff recordings: A theoretical approach," *IEEE Trans. Biomed. Eng.*, vol. 47, pp. 1281–1284, Sept. 2000.

[15] M. S. Rahal, "Optimization of nerve-cuff electrode recordings for functional electrical stimulation applications," Ph.D. dissertation, Dept. Electron. Elect. Eng., University College London, , London, U.K., 2000.

[16] E. Kreyszig, *Advanced Engineering Mathematics*, 8th ed. New York: Wiley, 1998.

[17] *The Current-Mode Approach*, C. Toumazou, D. Haigh, and J. Lidgey, Eds., IEE, London, U.K., 1990.

[18] R. Rieger, J. Taylor, A. Demosthenous, N. Donaldson, and P. Langlois, "Design of a low-noise preamplifier for nerve-cuff electrode recording," *IEEE J. Solid State Circuits*, vol. 38, pp. 1373–1379, Aug. 2003.

[19] A. Nedungadi and T. R. Viswanathan, "Design of linear CMOS transcondactance elements," *IEEE Trans. Circuits Syst.*, vol. CAS-31, pp. 891–894, Oct. 1984.

[20] K. Bult and H. Wallinga, "A class of analog CMOS circuits based on the square-law characteristic of an MOS transistor in saturation," *IEEE J. Solid-State Circuits*, vol. SC-22, pp. 357–365, June 1987.

[21] H. Träff, "Novel approach to high-speed CMOS current comparators," *Electron. Lett.*, vol. 28, pp. 310–312, Jan. 1992.

[22] R. Rieger, A. Demosthenous, and J. Taylor, "Continuously tunable, very long time constant integrator for a neural recording implant," in *Proc. 29th Eur. Solid-State Circuits Conf.*, Estoril, Portugal, 2003, pp. 441–444.

[23] "$0.8\ \mu$m CMOS process parameters," AustriaMicroSystems (AMS) Int. AG, Graz, Austria, Doc. 9 933 006, Rev. B ed., 1997.

Andreas Demosthenous (S'96–M'99) was born in Nicosia, Cyprus, in 1969. He received the B.Eng. degree in electrical and electronic engineering the M.Sc. degree in telecommunications technology, and the Ph.D. degree in electronic and electrical engineering from the University of Leicester, Leicester, U.K., the Aston University, Birmingham, U.K., and University College London (UCL), London, U.K., in 1992, 1994, and 1998, respectively.

From 1998 and 2000, he was a Postdoctoral Research Fellow in the Department of Electronic and Electrical Engineering, UCL, where, in September 2000, he was appointed a Lecturer. His main area of research is analog and mixed-signal integrated circuits for biomedical, digital communications, and signal-processing applications.

John Taylor (M'88) was born in Wanstead, U.K., in 1952. He received the B.Sc. and Ph.D. degrees from Imperial College, London, U.K., in 1973 and 1984, respectively.

During 1984–1985, he was a Research Fellow in the Department of Electrical Engineering, University of Edinburgh, Edinburgh, Scotland, where he worked on certain theoretical aspects of switched-capacitor filter design. He was a Reader in the Department of Electronic and Electrical Engineering, University College London (UCL), London, U.K. from 1985 to 2002. He was appointed the Chair of Microelectronics and Optoelectronics, University of Bath, Bath, U.K., in 2002. His research interests are in the field of analog integrated circuit and system design, including switched-capacitor filters, high-speed analog-to-digital converters (using electrooptic methods), convolutional decoders, and low-power implantable systems for biomedical and rehabilitation applications. He has published more than 100 technical papers in international journals and conferences and has coedited a handbook on filter design.

Iasonas F. Triantis was born in Geneva, Switzerland, in 1976. He received the M.Eng. degree from the Department of Electrical Engineering and Electronics, University of Manchester Institute of Science and Technology (UMIST), Manchester, U.K., in 2000. He is currently working toward the Ph.D. degree at University College London (UCL), London, U.K.

Between 2000 and 2003, he was a Research Assistant in the Department of Electronic and Electrical Engineering, UCL. His main research interests include analog integrated-circuit design and medical electronics for implanted devices.

Robert Rieger (S'01) was born in Duesseldorf, Germany, in 1975. He received the intermediate diploma in electrical engineering and the B.Eng. degree in electrical and electronics engineering from Chemnitz University of Technology, Chemnitz, Germany, and University of Kent, Canterbury, U.K., in 1998 and 2000, respectively. He is currently working toward the Ph.D. degree at the University College London (UCL), London, U.K.

Since November 2000, he has been a Research Assistant with UCL. His current research interests are in the area of low-power integrated circuits and systems with emphasis on biomedical applications.

Mr. Rieger is a student member of the German Association of Electrical Engineers (VDE).

Nick Donaldson received the doctoral degree in engineering and electrical sciences from Cambridge University, Cambridge, U.K..

From 1977 to 1992, he worked for the Medical Research Council, Neurological Prostheses Unit, London, U.K., under the direction of Prof. G.S. Brindley, working on the technology and use of implanted devices for the restoration of useful leg function to paraplegics. Since 1992, he has been Head of the Implanted Devices Group at University College London, London, U.K. He has been Principal Investigator for many projects related to implanted devices and functional electrical stimulation, and is currently also a Professor. His research interests now includes the development of implanted devices that use natural nerve signals as inputs, especially for preventing incontinence; stimulators of nerve roots; the use of electrical stimulation for recreational exercise of paralyzed legs; and methods to encourage functional neurological recovery after injury.